Non-intrusive load monitoring using high-frequency measurements and machine learning

Farid Dinar[1,2], Anis Harhoura[2], Sébastien Paris[2], Éric Busvelle[2,3], and Romain Chayla[1]

[1]INDEWATT, Pépinière #Cleantech, Avenue Louis Philibert, 13545 Aix-en-Provence, France
[2]LIS, UMR CNRS 7020, Université de Toulon, Aix Marseille Univ., France
[3]IUT de Toulon, Electrical Engineering and Computer Science Dept, Av. de l'Université, 83130 La Garde

ABSTRACT

Non-intrusive load monitoring can be considered as a knapsack or blind source separation problem, complicated by numerous possible combinations of devices that reconstruct total power. Simultaneous appliance usage and the presence of noise further complicate the task of accurately disaggregating the total power consumption into individual appliance contributions. In this paper we aim to solve the inverse problem of disaggregating the active power of each individual appliance from the overall power consumption and current harmonics. Additionally, we compare the performance of random forest, convolutional neural networks, support vector machine and linear regression models on the same set of features.

I. INTRODUCTION

Non-intrusive load monitoring (NILM), also known as energy disaggregation, has emerged as a promising technology for enhancing energy efficiency and promoting sustainable consumption in residential settings. Previous studies have shown that informing users about the energy consumption of household appliances can lead to a reduction in total consumption by up to 15% ([29]). As smart grids continue to evolve and electricity demand from households increases, NILM offers a powerful tool for both utility companies and consumers to gain detailed insights into energy usage patterns without the need for intrusive device-level monitoring [1], [5]. At its core, NILM aims to disaggregate the total electricity consumption of a household into individual appliance-level usage by analyzing the aggregate power signal from a single point of measurement, typically a smart meter [3]. This approach presents several advantages over traditional intrusive monitoring methods that require individual sensors for each appliance. NILM reduces hardware costs, simplifies installations and provides a scalable solution for widespread adoption in residential energy management systems [7]. The concept of NILM was first introduced in the 1980s, but recent advancements in machine learning, artificial intelligence, and the proliferation of smart meter data have reinvigorated research in this field. Modern NILM algorithms leverage sophisticated techniques such as deep neural networks, hidden Markov models, and various statistical methods to identify and classify the unique electrical signatures of different household appliances [9]. The potential applications of NILM are vast and multifaceted. For utility companies, NILM can provide valuable insights into consumer behavior, enabling more accurate load forecasting, demand response optimization, and personalized energy-saving recommendations. For consumers, NILM offers a detailed breakdown of their energy consumption, empowering them to make informed decisions about their usage habits and identify opportunities for conservation [6]. However, the implementation of NILM systems faces several challenges. These include the complexity of accurately disaggregating multiple overlapping appliance signatures, dealing with the variability in appliance characteristics across different households, and addressing privacy concerns related to the collection and analysis of high-resolution energy data [2], [8]. Recent research has focused on developing more robust and accurate NILM algorithms that can handle these challenges. Approaches such as federated learning have been proposed to address privacy concerns while still enabling personalized models [1]. Unsupervised learning techniques are being explored to reduce the need for labeled training data, making NILM systems more adaptable to new environments [8]. Additionally, hybrid models combining different machine learning architectures, such as convolutional neural networks (CNNs) and long short-term memory (LSTM) networks, have shown promise in improving disaggregation accuracy [5], [7]. The integration of NILM with other smart home technologies and the Internet of Things (IoT) presents exciting opportunities for creating more comprehensive and intelligent energy management systems. By combining NILM with smart thermostats, home automation systems, and renewable energy sources, it becomes possible to optimize energy usage in real-time, balancing comfort, cost, and environmental impact [4].

While traditional NILM approaches have focused on low-frequency sampling, recent advancements in high-frequency sampling techniques have opened new paths for more accurate and detailed load identification. High-frequency NILM leverages the rich information contained in transient signals and harmonic content, which are only accessible at higher sampling rates. This approach offers several advantages over low-frequency methods, including improved detection of appliance state changes, better discrimination between similar loads, and the ability to capture short-duration events [12], [17]. As a result, high-frequency NILM has the potential

to significantly enhance the accuracy and granularity of energy disaggregation. The development of high-frequency NILM systems presents unique challenges and opportunities. These include the need for advanced signal processing techniques, feature extraction methods tailored to high-frequency data, and machine learning algorithms capable of handling the increased complexity and volume of information [14], [18]. Additionally, researchers must address practical considerations such as data storage, computational requirements, and the potential for on-site disaggregation to reduce bandwidth and infrastructure demands [13]. Recent studies have explored various approaches to high-frequency NILM, including the use of discrete wavelet transforms for feature extraction, convolutional neural networks for transient classification [12], and graph signal processing for load identification [20]. These methods have demonstrated promising results in improving the accuracy and efficiency of load monitoring systems.

The interest of high-frequency NILM is not limited to detecting the start and stop sequences of electrical devices. It is also a way to characterize devices based on their internal electrical circuits. Spectral analysis (whether done using Fourier or wavelets) reveals a signature that will allow distinguishing a motor from a lamp with a dimmer, a power supply from a halogen lamp, or a refrigerator from a desktop ([24]). The presence of certain harmonics, and their absence, are particularly important elements, and spectral analysis has demonstrated its effectiveness in many fields for characterizing components from an aggregated measurement: chemistry, astronomy, marine acoustics... The reason is very clear: if, when several stationary sources overlap, the aggregated measurement is the sum of the signals, then the Fourier transform, due to its linearity, is the sum of the Fourier transforms. The problem of source separation becomes a very simple linear problem to solve, and the respective power of the sources can be calculated by simply inverting a linear system. In our case, it should therefore be very simple to detect the classes of devices that are on and their number in each class, as long as the classes of devices have a characteristic signature. In practice, two devices of the same nature do not necessarily have the same signature, and this is where classification by machine learning comes into play.

This article is an illustration of this remark. We plan to write a longer paper that will demonstrate the value of our approach in comparison with other methods, using a dataset available to researchers working on NILM (UK-Dale, [22], [23], see [24] for a discussion concerning other datasets). In this article however, we will work with data acquired by our own electronic board. In the first part, we will therefore present the board used and the conditions of signal acquisition (Section II), then in the second part, we will detail the algorithm used (Section III). Finally, we will show the results obtained (Section IV).

II. The board

The project we are working on is the result of collaboration with the company INDEWATT Sunleavs that has developed its own data logger which is currently being finalized. For this work, we used a commercially available board (IPEM ESP32E ATM90E36 SDK PCB, [26], see Fig. 1), that is based on the ATMEL component, the ATM90E36, coupled with an ESP32. This card proved to be more adequate than the current version of our board because it has an embedded ATM90E36 rather than an ATM90E32 which allows us to collect the current harmonics on three channels in addition to more conventional parameters like the current, the tension, and the powers. A new version of the company's board containing an ATM90E36 is currently being developed.

The ATM90E36 can sample the voltage and current at a frequency of 8 kHz (see [28], 7.1 p 39) and recover the sampled signal by DMA. The ESP32 reads these harmonic components along with fundamental measurements such as IRMS, VRMS, Apparent Power, Active Power, and Power Factor, subsequently transmitting the data to the serial port (1). A Python program then functions as a data logger, reading the serial port via USB, processing the data, and formatting it at intervals of one data point every two seconds. It is then sufficient to calculate the FFT of the signal over half a second, to obtain the spectrum and deduce the harmonics (real part and imaginary part). This FFT can be implemented on the ESP32. However, for this experience we use the ATM90E36 registers that, in addition to the apparent, active and reactive powers, and power factor, provide harmonic modules. Indeed, the ATM90E36A features a Discrete Fourier Transform (DFT) engine capable of calculating the 2nd to 32nd order harmonic components and the fundamental values for both voltage and current of each phase within the same period (see [28], 3.6, p18). We can therefore read these registers with the ESP32 and directly access the desired harmonics, an option that we took for reasons of simplicity (at a price that we will discuss later).

The IPEM board allows us to access to all functionalities of the ATM36, and therefore to measure the actual consumption of two devices at the same time. Using a second board, it is possible to measure up to four devices in addition to the main line current and voltage (we still use one channel on each board to measure the current on the main line, in order to ensure synchronization between the two boards during post-processing). Up to three SCT013 current clamps can be utilized to measure current consumption across three phases (Fig. 1, **A**). Allowing us to monitor two devices at the same time and their total consumption. Voltage measurement is performed using the Greenbrook DAT01A bell transformer (a simple 220V to 12V transformer, see [26]), which also powers the sensor (Fig. 1, **C**).

To summarize and to introduce some notations, the IPEM data logger gives us I_{RMS}, V_{RMS}, $\cos\varphi$, active and apparent power P_{active} and $P_{apparent}$, and current harmonics from h_1 (fundamental) to h_{32} from which we used only h_1, h_2 and odd harmonics up to fifteenth : h_3, h_5, h_7, h_9, h_{11}, h_{13} and h_{15} (see [24] for some comments on this choice of harmonics).

Fig. 2 shows the block diagram of our data logger.

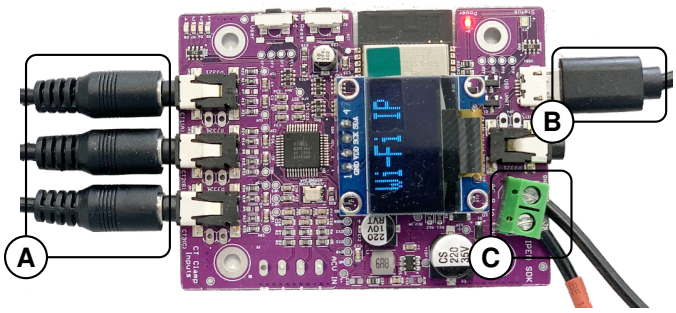

Fig. 1. IPEM board : **A** CT-013-00 current transformer inputs, **B** To PC via serial-USB **C** 12 V AC Input,

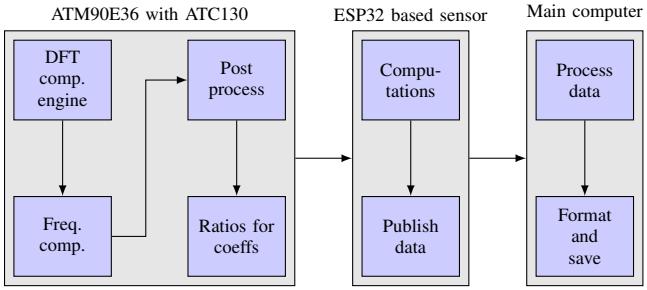

Fig. 2. Block diagram of the data logger

III. Experiments

A. Point-to-point

In the stationary case, the NILM problem based on the power and the power factor alone is an ill-posed problem, as soon as the number of possible sources that we wish to separate is greater than two. Even taking into account the chronological aspects, including the start and stop sequences (event-based NILM), it will therefore be very difficult to separate the devices based on these measurements alone. In contrast, harmonics provide relevant information that can help distinguish devices based on their signature in the frequency domain. We can verify this very simply, since in the stationary case, also designed by point-to-point approach, the NILM is an inversion problem of a linear system.

When mains voltage is applied to a device of type j (j being a lamp, a toaster, an iron, or any other type of devices), the current flowing through it is generally periodic (if the device has linear behavior) of the same period, but unless the device is purely resistive, a phase shift and harmonics appear. If the device has a stationary behavior (invariant over time), these harmonics characterize the shape of the current and therefore, to a certain extent, characterize the device (and those which have a very similar electrical circuit, which can be put in the same class). Let $H_j \in \mathbf{R}^n$ denote the vector made up of the first n harmonics (including the fundamental). We will denote by H the vector of harmonics measured on the total line. By linearity of the Fourier transform and according to the distance of the nodes, we have

$$\sum_{j=1}^{A} \alpha_j(t) H_j = H(t) \tag{1}$$

where for each device j, assuming that there are A appliances, α_j is an integer which represents the number of devices of type j in operation at time t.

This linear equation in α is a system of n equations with p unknowns which therefore admits a unique solution if $n \geq p$ and if the harmonics form a free system in $\mathbf{R}^n$. If each device consumes an apparent power P_j and P is the total apparent power, we will also have $\sum_{j=1}^{A} \alpha_j(t) P_j = P(t)$. This is a very rudimentary way of doing NILM, but it illustrates the principle of high frequency NILM.

We recorded all the parameters indicated in the previous section for four devices : a coffee maker, an iron, a hair dryer and a fan heater that operated intermittently for one hour, with a sampling time of two seconds (so we obtain 1800 samples, see Figs 4 to 8). We also recorded the total voltage and current. In this example, the goal is therefore to find the power consumed by each individual appliance as a function of time, based only on the measurements of the total line.

Firstly, and in order to illustrate our point, we will determine the signature of each device. Let us consider the measurements of the harmonics $(h_2(k), h_3(k), h_5(k), h_7(k), h_9(k), h_{11}(k), h_{13}(k), h_{15}(k)) \in \mathbf{R}^8$, $t = 1, \ldots, 1800$ (in this part, we only used harmonics and not powers (active or apparent) nor the power factor, in order to focus on the non-linearities of the devices). Among these 1800 samples, we only keep those 48 samples when coffee maker is on and we compute the average of each harmonic among these points. We note $h_{\text{coffee maker}} \in \mathbf{R}^8$ this average point. We obtain a characteristic spectrum of coffee maker. We do the same with the iron (65 samples), the hair dryer (349 samples) and the fan heater (419 samples), we obtain the signatures h_{iron}, $h_{\text{hair dryer}}$ and $h_{\text{fan heater}}$.

Figure 3 shows the result on the two principal axes of a principal component analysis. Each mark represents one measurement among the 1800 measurements taken during the 60 minutes of the experiment. The four circles materialize the signatures of the coffee maker, the iron, the hair dryer and the fan heater. We see that many measurements fall into these disks. These measurements correspond to times when only one device is on. Several points are close to 0 and correspond to times when no device is in operation. Other cluster of points corresponds to moments when several devices are working simultaneously (for instance, the cluster located on the northwest corresponds to time when the iron and the fan heater are on, other devices being off). If we had used the complex values of the harmonics, this cluster of points should be more accurately grouped around the sum of the signatures of the working devices (even after projection on the main axes of the PCA). However, the ATMEL component only gives us the modules of the harmonics which explains that the cluster is not exactly

located on the vector sum of the signatures. Finally, we note the presence of a few isolated points. Some correspond to the delay (of duration less than the sampling time which is 2 seconds) between the recording of a sample for the calculation of harmonics and the calculation of the active power which decides whether a device is in operation or not. Others correspond to the starting or stopping of a device, the harmonics then being calculated on a non-stationary signal and therefore not corresponding to the signature of one or the other of the two devices.

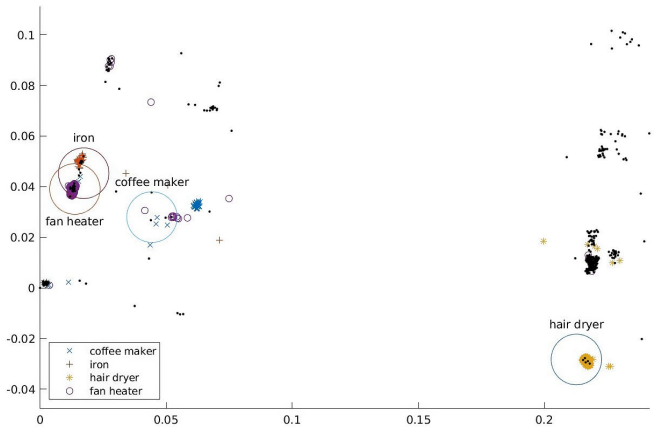

Fig. 3. Signature and measurements of devices on principal axis of a PCA

Figure 4 shows the evolution of the active power during the experiment. In addition to the power, we also measured, with the same frequency, the harmonics of the total current. At each moment, we solved the system 1 and obtained $\alpha_{\text{coffee maker}}(t)$, $\alpha_{\text{iron}}(t)$, $\alpha_{\text{hair dryer}}(t)$ and $\alpha_{\text{fan heater}}(t)$ as a function of time. These two parameters allow us to calculate the active powers of each device as a function of time, $P_{\text{a}}(t) = \bar{P}_{\text{a}}\alpha_{\text{a}}(t)$, where $\bar{P}_{\text{a}}$ are the average apparent powers of the appliances in $\{\text{coffee maker}, \text{iron}, \text{hair dryer}, \text{fan heater}\}$.

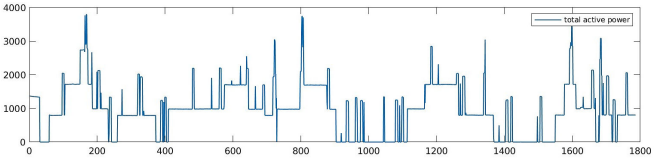

Fig. 4. Total apparent power

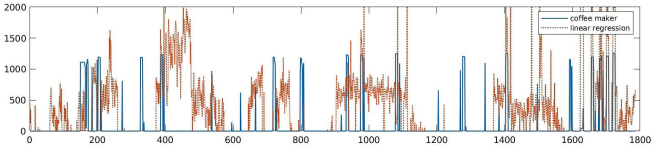

Fig. 5. Coffee maker power

We obtain the regressions shown on Figures 5, 6, 7 and 8. Several remarks can be made. First of all, the only result that can be considered correct is the regression of the active

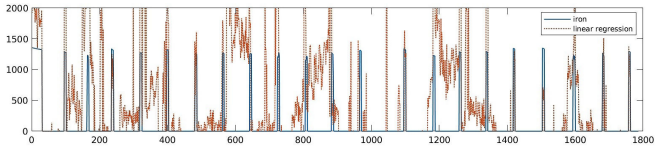

Fig. 6. Iron power

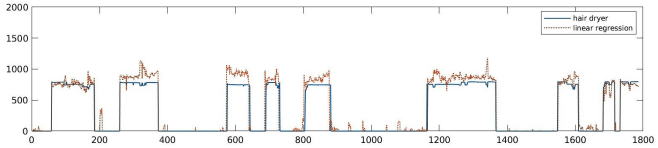

Fig. 7. Hair dryer power

power of the hair dryer. This is not a coincidence, we can indeed see on the figure 3 that the signature of the hair dryer is clearly distinguished from the other signatures, on the first axis of the principal component analysis. For this same reason, we note that the confusions between the iron and the fan heater are numerous and makes the method totally ineffective. We will see that the non-linear methods but especially sequence-to-point rather than point-to-point perform obviously better.

B. Sequence-to-point

In this paper, we utilize the Seq2Point methodology specifically to predict the mid-sequence point, effectively capturing temporal dependencies in power consumption data. By using a sequence length of 30 samples, corresponding to one minute, Seq2Point successfully captures sequential patterns. This approach significantly improves the prediction of devices power usage on unseen data compared to the point-to-point method, which treats each measurement independently.

To formalize this, let A represent the total number of household appliances, indexed by i where $i = 1, \ldots, A$. The overall power consumption at any time t, denoted by $P(t)$, and $p_i(t)$ for $i = 1$ to A the power consumed by each appliance i at moment t. In NILM, the relationship at time t can be described by the equation:

$$P(t) = \sum_{a=1}^{A} P_a(t)$$

Initially, we began by exploring standard methods to set a performance baseline, eliminating other methods that did not perform as well, and then trained a random forest using our selected features. As parameter optimization techniques are not included in this study, we manually adjust the random

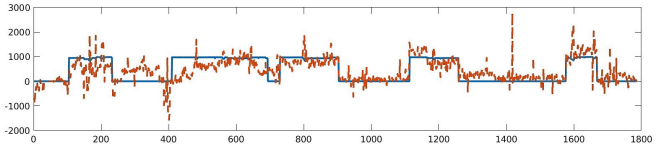

Fig. 8. Fan heater power

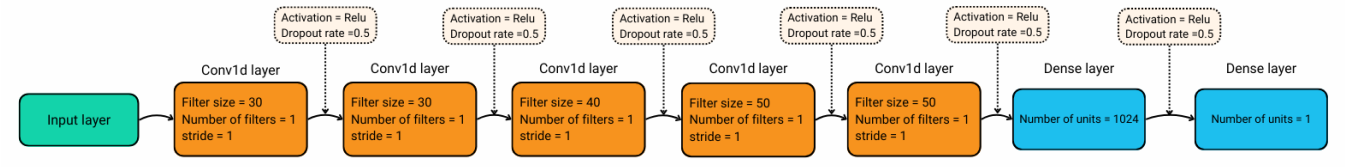

Fig. 9. The proposed architecture for the convolutional neural networks.

forest parameters to improve performance. The proposed CNN model is inspired from [25], which consists of five convolutional layers with ReLU activation, and to improve regularization and prevent overfitting, we added a dropout layer on top of both the convolutional and fully connected layers. This is followed by fully connected layers to produce the regression output. The model is trained using the Adam optimizer and Mean Squared Error loss function. The detailed architecture is illustrated in figure 9. The performance of a NILM system, especially in regression tasks, is typically evaluated using metrics such as Mean Absolute Error (MAE), which measures the average prediction error in Watts, Mean Relative Error (MRE), which normalizes the error relative to actual values, and Mean Squared Error (MSE), which gives more weight to larger errors by squaring them. The goal is to quantify the divergence of the predicted power from the corresponding real one. These errors are described by the equations, where N is the length of the predicted sequence, $\hat{p}_i$ is the estimated electrical power consumption, and p_i is the true value of active power consumption at the moment t:

$$MAE = \frac{1}{N}\sum_{i=1}^{N}|\hat{p}_i - p_i| \tag{2}$$

$$MRE = \frac{1}{N}\sum_{i=1}^{N}\frac{|\hat{p}_i - p_i|}{|p_i|} \tag{3}$$

$$MSE = \frac{1}{N}\sum_{i=1}^{N}(\hat{p}_i - p_i)^2 \tag{4}$$

IV. Our results

To evaluate our proposed approach, we conducted experiments using data provided by the two sensors described in section III. The dataset spans one hour long and sampled at a 2 seconds rate. The trained models were tested on the same unseen portion of the dataset. The experimental results for the hairdryer, iron, coffee maker, and the fan are presented in Table I. These results clearly indicate that the Random Forest model consistently outperforms the other approaches across the various metrics for the tested appliances.

Figures 10, 11, 12 and 13 further illustrate this by comparing the ground truth with the predictions of the active power for the studied appliances over the same period using the different models. Overall, the Random Forest model accurately captured the power consumption patterns for the hairdryer and iron, but performed slightly worse for the coffee maker and fan. The CNN model also demonstrated a strong performance in detecting the start and the end of each

Target	Model	MRE ↓	MAE ↓	MSE ↓
Hairdryer	Random Forest	**0.003**	**2.69**	**204.40**
	SVM	0.34	275.74	173028
	Linear Regression	0.04	35.80	2716
	CNN	0.91	238.01	138402
Iron	Random Forest	**0.04**	**62.55**	**43106**
	SVM	0.06	94.37	118298
	Linear Regression	0.12	167.54	64426
	CNN	0.97	78.87	68647
Coffee maker	Random Forest	**0.08**	**113.03**	**105823**
	SVM	0.09	125.27	142712
	Linear Regression	0.18	239.43	114440
	CNN	0.96	122.34	101644
Fan	Random Forest	**0.03**	**33.10**	**21343**
	SVM	0.48	482.36	279634
	Linear Regression	0.11	157.04	43300
	CNN	0.93	223.32	140698

TABLE I

Performance metrics for different models

device's usage but struggled with accurately estimating the power consumption, performing comparably to the Random Forest for some appliances. In contrast, the SVM model struggled, especially with the iron and coffee maker data (which have close signatures, see Fig. 3 and which have the same usage pattern over time, see Figs. 5 and 6), showing significant deviations and almost flat predictions in several segments. These results suggest that Random Forest and CNN are better suited for predicting appliances power consumption in this dataset, with Random Forest being the superior model. The superior performance of RF can be attributed to several factors. First, the dataset used in this study was limited to one hour of data, sampled at a 0.5 Hz rate, providing fewer than 1800 data points per appliance. Such a small dataset can significantly limit the ability of complex models like CNNs to generalize well, as they typically require larger datasets to capture intricate patterns effectively. In contrast, Random Forests can perform relatively well even with smaller datasets due to their ensemble nature, which reduces the risk of overfitting. Additionally, RFs are relatively less complex compared to CNNs, as they operate by constructing multiple decision trees during training and outputting the mean prediction of the individual trees. This simplicity allows them to perform well even with limited data, whereas the high complexity of CNNs, with their multiple layers and parameters, might not be fully leveraged with the given data size. To fully leverage the potential of CNNs and other complex models, future work should include larger datasets, automated hyperparameter optimization techniques, advanced feature extraction methods, and possibly hybrid

approaches that combine the strengths of different models.

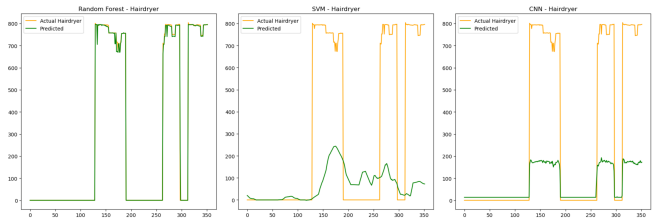

Fig. 10. Hairdryer usage prediction by different models

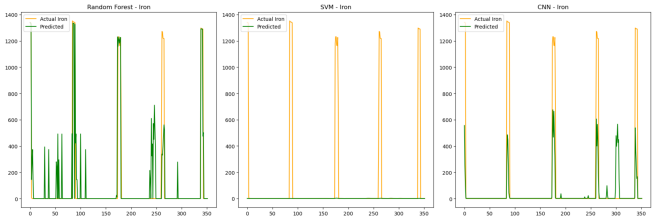

Fig. 11. Iron usage prediction by different models

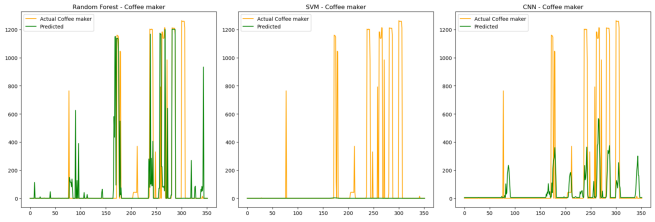

Fig. 12. Coffee maker usage prediction by different models

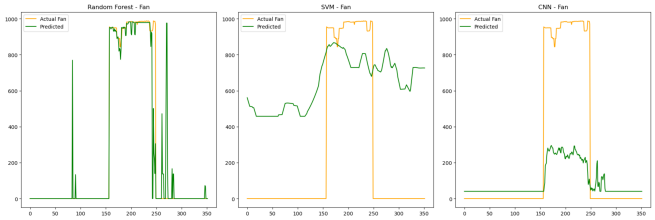

Fig. 13. Fan usage prediction by different models

V. Conclusion

This work is the result of collaboration between the LIS laboratory (AMU, Toulon) and the company Indewatt. The project is called SunLeavs. A board was developed by the company Indewatt, which initially used the ATM90E32 component. We have upgraded this board to the ATM90E36 component, which allows high-frequency acquisition. It integrates a DSP that calculates the magnitudes of the harmonics up to the 32nd. It also enables acquisition via DMA, which will later allow for the calculation of the real and imaginary parts of the harmonics, in order to exploit the linearity of the transformation (which is not the case with spectral power).

References

[1] Wang, Xuan, Zebang Zhang, and Qiang Yang. "Federated Learning based Non-Intrusive Load Monitoring in Domestic Energy Systems." In 2023 IEEE 7th Conference on Energy Internet and Energy System Integration (EI2), pp. 2201-2207. IEEE, 2023.

[2] Zhou, Zejian, Yingmeng Xiang, Hao Xu, Yishen Wang, and Di Shi. "Unsupervised learning for non-intrusive load monitoring in smart grid based on spiking deep neural network." Journal of Modern Power Systems and Clean Energy 10, no. 3 (2021): 606-616.

[3] Wang, Xiaojing, Dongmei Lei, Jing Yong, Liqiang Zeng, and Sam West. "An online load identification algorithm for non-intrusive load monitoring in homes." In 2013 IEEE Eighth International Conference on Intelligent Sensors, Sensor Networks and Information Processing, pp. 1-6. IEEE, 2013.

[4] Sun, Ruichen, Kun Dong, and Jianfeng Zhao. "DiffNILM: a novel framework for non-intrusive load monitoring based on the conditional diffusion model." Sensors 23, no. 7 (2023): 3540.

[5] Zai, Zhoupeng, Sheng Zhao, Zhengjiang Zhang, Haolei Li, and Nianqi Sun. "Non-intrusive load monitoring based on the combination of gate-transformer and CNN." Electronics 12, no. 13 (2023): 2824.

[6] Du, Zhekai, Jingjing Li, Lei Zhu, Ke Lu, and Heng Tao Shen. "Adversarial Energy Disaggregation for Non-intrusive Load Monitoring." arXiv preprint arXiv:2108.01998 (2021).

[7] Laouali, Inoussa, Antonio Ruano, Maria da Graça Ruano, Saad Dosse Bennani, and Hakim El Fadili. "Non-intrusive load monitoring of household devices using a hybrid deep learning model through convex hull-based data selection." Energies 15, no. 3 (2022): 1215.

[8] Criado-Ramón, David, Luis G. Baca Ruíz, J. R. S. Iruela, and M. C. Pegalajar. "A Novel Non-Intrusive Load Monitoring Algorithm for Unsupervised Disaggregation of Household Appliances." Information 15, no. 2 (2024): 87.

[9] Devlin, M., and Hayes, B. P. (2019, August). Non-intrusive load monitoring using electricity smart meter data: A deep learning approach. In 2019 IEEE Power & Energy Society General Meeting (PESGM) (pp. 1-5). IEEE.

[10] Pihala, H. (1998). Non-intrusive appliance load monitoring system based on a modern kWh-meter.

[11] Fang, Z., Zhao, D., Chen, C., Li, Y., and Tian, Y. (2020). Nonintrusive appliance identification with appliance-specific networks. IEEE Transactions on Industry Applications, 56(4), 3443-3452.

[12] Chang, Hsueh-Hsien, Heng-Jui Chang, and Ching-Lung Lin. "Novel High-Frequency Transient Techniques in Non-Intrusive Load Monitoring Techniques." In 2023 8th Asia Conference on Power and Electrical Engineering (ACPEE), pp. 1533-1538. IEEE, 2023.

[13] Kotsilitis, Sarantis, Emmanouil Kalligeros, Eftychia C. Marcoulaki, and Irene G. Karybali. "An efficient lightweight event detection algorithm for on-site non-intrusive load monitoring." IEEE Transactions on Instrumentation and Measurement 72 (2022): 1-13.

[14] Nour, Mohamad, Jean-Charles Le Bunetel, Philippe Ravier, and Yves Raingeaud. "Data augmentation strategies for high-frequency NILM datasets." IEEE Transactions on Instrumentation and Measurement 72 (2023): 1-9.

[15] Gopinath, Rajendiran, Mukesh Kumar, C. Prakash Chandra Joshua, and Kota Srinivas. "Energy management using non-intrusive load monitoring techniques–State-of-the-art and future research directions." Sustainable Cities and Society 62 (2020): 102411.

[16] Timplalexis, Christos, Georgios-Fotios Angelis, Stelios Krinidis, Dimosthenis Ioannidis, and Dimitrios Tzovaras. "Low frequency residential non-intrusive load monitoring based on a hybrid feature extraction tree-learning approach." Energy Sources, Part A: Recovery, Utilization, and Environmental Effects 44, no. 1 (2022): 493-514.

[17] Guzmán, Ian, Keith Goossen, and Kenneth Barner. "Classification of high frequency NILM transients based on convolutional neural networks." In 2022 IEEE Green Energy and Smart System Systems (IGESSC), pp. 1-6. IEEE, 2022.

[18] Kang, Ju-Song, Miao Yu, Lingxia Lu, Bingnan Wang, and Zhejing Bao. "Adaptive non-intrusive load monitoring based on feature fusion." IEEE Sensors Journal 22, no. 7 (2022): 6985-6994.

[19] Shi, Jiachuan, Dingrui Zhi, and Rao Fu. "Research on a Non-Intrusive Load Recognition Algorithm Based on High-Frequency Signal Decomposition with Improved VI Trajectory and Background Color Coding." Mathematics 12, no. 1 (2023): 30.

[20] Li, Xuhao, Bochao Zhao, Wenpeng Luan, and Bo Liu. "A training-free non-intrusive load monitoring approach for high-frequency measurements based on graph signal processing." In 2022 7th Asia Conference

on Power and Electrical Engineering (ACPEE), pp. 859-863. IEEE, 2022.

[21] Leksono, Edi, Auditio Mandhany, Irsyad Nashirul Haq, Justin Pradipta, Putu Handre, Kertha Utama, Reza Fauzi Iskandar, and Rezky Mahesa Nanda. "Development of Non-Intrusive Load Monitoring of Electricity Load Classification with Low-Frequency Sampling Based on Support Vector Machine." Journal of Engineering and Technological Sciences 55, no. 2 (2023).

[22] Kelly, Jack, and William Knottenbelt. "The UK-DALE dataset, domestic appliance-level electricity demand and whole-house demand from five UK homes." Scientific data 2, no. 1 (2015): 1-14.

[23] Sykiotis, Stavros, Maria Kaselimi, Anastasios Doulamis, and Nikolaos Doulamis. "Electricity: An efficient transformer for non-intrusive load monitoring." Sensors 22, no. 8 (2022): 2926.

[24] Dinar, Farid, Romain Chayla, Sébastien Paris, and Eric Busvelle. "A low-level set of stationary features dedicated to non-intrusive load monitoring." In 2022 10th International Conference on Systems and Control (ICSC), pp. 435-441. IEEE, 2022.

[25] Zhang, C., Zhong, M., Wang, Z., Goddard, N., & Sutton, C. (2018, April). Sequence-to-point learning with neural networks for non-intrusive load monitoring. In Proceedings of the AAAI conference on artificial intelligence (Vol. 32, No. 1).

[26] IPEM ESP32E ATM90E36 SDK, https://ditronix.net/

[27] ATM36 Application note (microchip.com), https://ww1.microchip.com/downloads/en/Appnotes/Atmel-46104-SE-M90E36A-%20ApplicationNote%20.pdf

[28] ATM36 Datasheet (microchip.com), https://ww1.microchip.com/downloads/en/DeviceDoc/Atmel-46004-SE-M90E36A-Datasheet.pdf

[29] Darby, Sarah. "The effectiveness of feedback on energy consumption." A Review for DEFRA of the Literature on Metering, Billing and direct Displays 486, no. 2006 (2006): 26.